Attempt to Classify the Microphone Array Deconvolution Methods in Aeroacoustics

Christophe Picard, Quentin Leclere

PROCEEDINGS of the
23rd International Congress on Acoustics

9 to 13 September 2019 in Aachen, Germany

Attempt to Classify the Microphone Array Deconvolution Methods in Aeroacoustics

Christophe PICARD[1]; Quentin LECLERE[2]

[1] MicrodB, France

[2] Laboratoire Vibrations Acoustique (LVA), University of Lyon, INSA-Lyon, France

ABSTRACT

In the field of experimental aeroacoustics in wind tunnel, the number of existing methods is important and is increasing continuously so that it becomes difficult for Industrials to have a clear view of the respective advantages of each of them and make appropriate choice. Benchmark works are also plentiful and often focus on the performance of these methods in terms of spatial localization and computing time, more rarely in terms of quantitative estimation. We are interested here by these deconvolution methods that we aim to classify, and even to show in what extent all of these methods are equivalent. The approach adopted is to define a common protocol for controlling and monitoring the different algorithms: define same initial condition, same convergence parameters and same exit conditions. All of the considered deconvolution algorithms are implemented with respect to the same protocol. Convergence and calculation time are monitored at each frequency. Finally acoustic power of source area are extracted from the resulting maps and compared together. Indeed, it is observed that within the range of few dBs the results are quite similar and we propose to classify the algorithms with their equivalent Lp-norm minimization function.

Keywords: Microphone array technique, Deconvolution, Aeroacoustics, Wind tunnel measurements, Airframe noise

1. INTRODUCTION

Aeroacoustic measurements based on acoustic arrays in wind tunnels can provide a detailed understanding of complex noise sources. In particular for airframe noise in aeronautics, wind tunnel tests help to investigate new aircraft concepts, verify performance of innovative designs and validate prediction models. Indeed, thanks to increasing computational power, more and more CFD models are used in design phases, and wind tunnel testing is the ultimate way to validate these models long before the aircraft can actually fly. However, wind tunnel testing is often very expensive and must be performed efficiently to get the most out of the limited testing time.

Microphone array techniques provide a considerable amount of data from which it is possible to extract valuable information on the origin of sound such as location or power of acoustic sources. The most common microphone array method is certainly the conventional beamforming algorithm (CBF [1], also known as “delay-and-sum” [2]) because of its simplicity, robustness and computational efficiency. However it suffers from a lack of resolution in the low frequency range and from the inability to properly quantify the source power, especially in the case of complex source distributions like those generally encountered in aeroacoustics. These drawbacks have been tackled in the 2000’s with advanced beamforming-based algorithms such as deconvolution techniques. In the field of experimental aeroacoustics in wind tunnel, the number of existing deconvolution methods is important (Clean-PSF [3], DAMAS [4], SEM [5], Clean-SC [6] and NNLS [7], and the many derived versions). All of these methods in fact share the same theoretical basis. Indeed the physical model is the same and the techniques only differ from the final inversion algorithm, while, in aeroacoustics, the model in general assumes an uncorrelated monopole distribution in free field [8].

We are interested here by these deconvolution methods that we aim to classify, and even to show

[1] christophe.picard@microdb.fr
[2] quentin.leclere@insa-lyon.fr

in what extent all of these methods are equivalent. The approach adopted is to define a common protocol for controlling and monitoring the different algorithms: define same initial condition, same convergence parameters and same exit conditions. The DLR1 case (Dornier-728 half model) [9] taken from the Array Analysis Benchmark [10] is used. All of the already mentioned deconvolution algorithms are implemented with respect to the same protocol. Convergence and calculation time are monitored at each frequency. Finally acoustic power of source area are extracted from the obtained maps and compared together. Indeed, it is observed that within the range of 1-2dB the results are quite similar and we propose to classify the algorithms with their equivalent Lp-norm minimization function.

2. MICROPHONE ARRAY TECHNIQUES

2.1 General principles

Many acoustic imaging techniques have been developed over the past 30 years. These techniques have in common the formalization of the theoretical problem which is to estimate the position and power level of acoustic sources from pressure measurements on a microphone array.

The principle of identifying sources consists in positioning a microphone array facing the object to study and try to locate the main noise areas through specific processing of microphone signals, based on a source model chosen *a priori*. For aeroacoustic applications, the usual hypothesis is to assume that the phenomena are well represented by a distribution of uncorrelated monopoles [8]. This can be justified by the fact that the pressure correlation scales are lower than the spatial resolution of the method in general. One then seeks the model adequacy to the measurement data.

One distinguishes far field and near field zones of the array (respectively Fraunhofer and Fresnel zones). It is admitted [8] that it is advantageous to measure a source in the near field of the array, in particular to overcome the background noise. The source emission is then spherical and one performs a focused array processing where the position of the source is sought, that is to say the emission center of the spherical wave. This model is the most commonly used (in aeroacoustics anyway) and usually provides interesting and useful results. But it must be noticed that this is an approximation of the propagation model and that the differences between the actual acoustic propagation and the propagation model can result in errors, especially on the source amplitudes.

In practice, one chooses a region of the scan area, where the presence of sources is sought for. For practical reasons linked to mechanical design, one generally arrange the microphones on a plane. For a typical 2D configuration, an area of candidate source points is then defined in a plane parallel to the microphone array.

2.2 Expression of the direct problem

By solving the wave equation in the frequency domain for a source in an open field and discretizing the solution, the complex pressure vector $\boldsymbol{P}$ $(M \times 1)$ received at the M microphones of the array at frequency f can be expressed as:

$$\boldsymbol{P} = \boldsymbol{G}_j q_j, \tag{1}$$

where q_j is the complex amplitude of a source at point $\boldsymbol{\xi}_j$ and $\boldsymbol{G}_j$ is the Green function vector $(M \times 1)$ in free space between the source and the microphones M at points $\boldsymbol{x}_i$, $i \in [1 \dots M]$. The frequency dependence of the equations is omitted in the notation of this paper.

In the presence of strong background noise perturbation, as often it is the case in aeroacoustics, it is wise to proceed with ensemble averages in the frequency domain, assuming stationarity property of signals. For this, one uses the cross spectral matrix (CSM) of the measured signals on the array, matrix of complex values, expressed as:

$$\boldsymbol{C} = \langle \boldsymbol{P}\boldsymbol{P}^* \rangle, \tag{2}$$

with $\langle \cdots \rangle$ designating the ensemble average and the superscript $\blacksquare^*$ being the Hermitian complex conjugate operator.

Applying this to equation (1), in the presence of S sources and assuming uncorrelated source model, i.e. incoherent sources, leads to the following expression of the modelled CSM:

$$\boldsymbol{C}_{mod} = \sum_{j=1}^{S} \boldsymbol{G}_j \boldsymbol{G}_j^* Q_j, \tag{3}$$

with Q_j being the power spectral density of the sources at each considered point $\boldsymbol{\xi}_j$. Methods considering other source models also exist, see [11] and [12] for a review.

2.3 Expression of the inverse problem

Starting from equation (3), the sound source identification consists in the estimation of the power spectral density of the sources knowing the measured CSM $\boldsymbol{C}_{mes}$ (measured pressure signals on the array). This is an inverse problem that can be solved using a classical optimization procedure. For that, an objective function - error function or cost function - is defined, traducing the adequacy of the model to the measurement data. A L2-norm is chosen here to quantify the difference between the measured CSM and the modelled CSM, i.e.:

$$\varepsilon = \|\boldsymbol{C}_{mes} - \boldsymbol{C}_{mod}\|^2 . \tag{4}$$

The objective is then to minimize this cost function by considering its gradient regarding the unknown, i.e. searching an estimation of unknown Q_j satisfying:

$$\frac{\partial \epsilon}{\partial Q_j} = 0 \text{ or } Q_j = 0, \text{ subject to } Q_j \geq 0 \text{ for all considered candidate source point } j. \tag{5}$$

All deconvolution methods intend to solve the optimization problem (5), or close forms of it. What differentiates them lies in the algorithms that are implemented to find a solution. The conventional beamforming method and general principles of deconvolution methods are presented hereafter.

2.4 Conventional Beamforming method

The most commonly used method in the industry for the identification of acoustic sources is the conventional beamforming (CBF) for which an estimate of the power spectral density is searched for each source point scanned one after the other among the chosen set of candidate points. This means considering the following modelled CSM :

$$\boldsymbol{C}_{mod} = \boldsymbol{G}_j \boldsymbol{G}_j^* Q_j. \tag{6}$$

Deriving the optimization procedure leads to the following estimate of the source power spectral density A_j at the considered scan point $\boldsymbol{\xi}_j$:

$$A_j = \boldsymbol{w}_j^* \boldsymbol{C}_{mes} \boldsymbol{w}_j, \tag{7}$$

where $\boldsymbol{w_j} = \boldsymbol{G}_j / \boldsymbol{G}_j^* \boldsymbol{G}_j$ is viewed as a spatial filter.

In the case of a unique real source at point $\boldsymbol{\xi}_j$, the linear regression determines A_j is the best estimation of the power spectral density of the real source [8].

2.5 Deconvolution methods

The conventional beamforming method suffers from severe limitations. The beamforming process in fact performs a spatial convolution between the true source distribution and the response of the array to a unique point source, called Point Spread Function, PSF, whose shape depends on the number of microphones, their spatial arrangement, the frequency and the relative position of the center of the array to the scan point. This generates artefacts as main lobes, side lobes and grating lobes that pollute the resulting source map. These non-physical artefacts may render physical interpretation difficult. The PSF at point $\boldsymbol{\xi}_j$ due to a source at point $\boldsymbol{\xi}_k$ can be expressed as:

$$\mathrm{R}_{jk} = \left(\boldsymbol{w}_j^* \boldsymbol{G}_k \boldsymbol{G}_k^* \boldsymbol{w}_j\right) = \left\|\boldsymbol{w}_j^* \boldsymbol{G}_k\right\|^2. \tag{8}$$

It is then possible to express the CBF result A_j as a product of the array directivity pattern R_{jk} and the true power spectral density Q_k:

$$A_j = \mathrm{R}_{jk} Q_k. \tag{9}$$

Considering a set of N candidate points the CBF map result, $(N \times 1)$ vector **A,** is expressed as the product of the complete PSF, i.e. $(N \times N)$ matrix **R**, and the $(N \times 1)$ vector of source candidates **Q,** thus forming a second linear system assuming incoherent sources (also called in the field as the DAMAS problem [4]):

$$\mathbf{A} = \mathbf{RQ}, \tag{10}$$

which requires a second inversion method of a linear system. The special feature of equation (10) thus obtained is that all terms of the system are real and positive. A positivity constraint thus has to be considered on the unknowns **Q**.

It is necessary to introduce here a quantity used in the optimization algorithm, called the residue and defined by :

$$\mathbf{r} = \mathbf{A} - \mathbf{RQ}. \tag{11}$$

It is interesting to note at this point that starting from equation (4) but considering all N scanned points at once, i.e. considering equation (3) for the modelled CSM instead of equation (6) (as for conventional beamforming), Blacodon and Elias [5] derived the optimization process (as shortly described in section 2.3), and resulted in the same linear system to be solve as equation (10).
A fundamental question arises about this problem. Indeed some consider a linear system and others a quadratic system (nonlinear), both under constraint, depending on considering the unknown vector $\mathbf{Q}$ as linear or as a quadratic quantity, what it is physically. This question has no answer within the community to our knowledge, and should have a consequence on the choice of solving algorithms.
Whatever, it is expected that the positivity constraint has a strong regularizing effect and tends to foster sparsity of the solution. Thus any algorithm used in applied mathematics should find equivalently a local minimum even without any penalty (regularization).

To overcome artefacts due to the directivity of the array, the deconvolution process consists in two steps: 1/ estimate the CBF result at each point of the chosen scan grid with equation (7) and 2/ estimate the source power density taking into account all the scanning points at the same time by solving equation (10), iteratively in general.

2.5.1 Approach adopted

For this study, we consider 5 deconvolution algorithms: Clean-PSF [3], DAMAS [4], SEM [5], NNLS [7] and CIRA [13]. Even if Clean-SC [6] is one of the most popular deconvolution methods in the field of aeroacoustics, it isn't considered here because it differs from the others in the sense that it modifies steering vector during the iterative process. Note that for SEM, the selected algorithm is a simple Conjugate Gradient (easier to modify) as chosen initially (CONMIN) and instead of LBFGS as finally proposed by the authors.

The implementation in an industrial context of this type of algorithm requires a lot of attention in particular with regard to the initial condition, the management of convergence and positivity constraint, and the exit conditions of the algorithm. Our experience is that the initial condition have no important impact on the convergence speed and the result, the final map. On the other hand management of convergence and exit conditions of the algorithm have a more crucial impact.

There are also other implementation tricks useful for aeroacoustics (CSM diagonal removal (DR), consideration of convection effects on acoustic propagation (Amiet)) that are actually applied in this work. Note that the DR option requires consistent operations to be applied in the algorithm, particularly with regard to the positivity constraint to be applied to the initial CBF map or to the positive matrix $\mathbf{R}$. All of these implementation details are not detailed in this publication.

After a literature revue on the methods and algorithms, the approach adopted, based on making compromise and synthesis, is to define a common protocol for controlling and monitoring the chosen algorithms during the different parts of a deconvolution algorithm:

- initial condition
  There's two options for the initial map (also called clean map in Clean-PSF): either set to zero or initialized by the CBF map, possibly renormalized. In the literature, the initial map is set to zero or to the CBF map. For all algorithms we choose here the first option for the sake of consistency between algorithms, because Clean-PSF algorithm can't support the other choice.
- management of convergence
  We are talking about the convergence parameter which can be called sometimes relaxation parameter, step factor, loop factor or energy injection factor, and about the positivity constraint.
  Convergence parameter is certainly the most delicate part to settle in this work because the chosen algorithms consider this kind of parameter in very different ways. SEM (CG) and NNLS contain a convergence parameter that is automatically calculated at each iteration. The convergence parameter for CIRA is defined once at each frequency but several options exist. And, finally, Dougherty proposed to integrate a convergence parameter in Clean-PSF to counteract somehow the spatial extent of aeroacoustic sources, parameter settled empirically (typically between 0.1 and 0.25). In the end, harmonization between algorithms is not feasible and we choose to apply the best/optimized know-how concerning the convergence parameter, for the algorithms that require a user defined choice.
  Imposition of positivity is an absolute necessity for our deconvolution methods. The most consistent option is to zero all negative solutions founded in the map at each iteration. It was possible to impose this constraint on all the algorithms chosen in this work.
- exit conditions of the algorithm

This is the most confusing part encountered in the bibliography or even the less well documented. There is no consensus on this issue. In summary we usually find two associated criteria for the exit of the algorithm: an energy criterion and a maximum number of iterations, a safety condition that sets the limit of the exit condition. In terms of energy criterion we can list non-exhaustively the following conditions. We then propose to evaluate in this work the following energy criteria at each iteration $\boldsymbol{i}$:

- the L0-norm of the resulting map (clean map), called here $L0n^{(i)}$,
- the L1-norm of the clean map, called here $L1n^{(i)}$. Note that because of the quadratic nature of the physical quantity to identify, this represents in fact the squared L2-norm of the source level in the map,
- the L2-norm of the clean map, called here $L2n^{(i)}$,
- the value of the cost function (equation (4) at iteration (i)) $\varepsilon^{(i)}$, eventually normalized by the energy in the CSM $\|\boldsymbol{C}_{mes}\|^2$, i.e. $N\varepsilon^{(i)} = \varepsilon^{(i)}/\|\boldsymbol{C}_{mes}\|^2$. A special care must be taken in case of DR option is selected, for the calculation of $\boldsymbol{C}_{mes}$,
- going back to the optimization procedure (§2.3), a local minimum can be founded when equation (5) is satisfied. In Fact equation (5) is equal to the residue (equation (11)), expressed in the iterative process as $\boldsymbol{r}^{(i)} = \mathbf{A} - \mathbf{RQ}^{(i)}$. Then the L2-norm of the residue, defined by $L2nr^{(i)} = \|\boldsymbol{r}^{(i)}\|$, can be used.

The question of defining a relevant threshold for each criteria then arise. Threshold values of energy criteria are often chosen empirically. To try to clarify this question, the solution adopted here is to observe also the evolution of the criteria between two successive iterations, i.e. for example $\left|\varepsilon^{(i)} - \varepsilon^{(i-1)}\right|$.

Reminding that it is expected to compare and classify the 5 algorithms, following a (as much as) common and global protocol, it seems necessary to consider also the industrial process of analyzing acoustic imaging results. Indeed, in general, engineers are interested in the integrated source power on areas related to components to optimize. That's why it is decided to monitor also the source power integrate in the following areas [9]: FLAP INT, SLAP INT and FLAP TIP. It defined finally all the criteria we have monitored in this study (next section).

All of the considered deconvolution algorithms are implemented with respect to the same pseudo-code.

2.5.2 *Modus operandi* adopted

The study is composed of two parts. Firstly the chosen algorithms will be monitored for several discrete frequencies: 2021Hz, 3018Hz, 4394Hz, 5010Hz, 6006Hz, 7002Hz and 8496Hz. A maximum number of iterations is fixed arbitrarily from 200 in the lowest frequency band to 100 in the highest) and the energy convergence criteria (previous section) are monitored at each iteration. The objective is to observe the behavior of each algorithm and try to identify the most relevant exit criteria for each algorithm, finding supposed local minima. Then, secondly, more complete calculation will be done in third octave bands and integrated energy on defined areas will be compared.

3. IMPLEMENTATION

3.1 Test case description

The test case selected here is the AIAA array analysis benchmark case DLR 1, Aircraft Half Model in closed wind tunnel. This benchmark problem consists of a test configuration with a Dornier-728 half model of scale 1:9.24 in high-lift configuration (landing) placed in the center of the cryogenic wind tunnel at the DLR Kryo-Kanal Koeln (DNW-KKK), refer to [9] and [10] for a more complete description of the test case.

The microphone array has a diameter of 1 m and is composed of 135 microphones arranged in spiral arms mounted onto the sidewall. The sampling frequency of microphone signals is 120 kHz.

The benchmark data is acquired for 9 couples of parameters: 3 model angles of attack (3°, 5° and 9°) and 3 free stream velocities (Mach numbers M=0.15, 0.2 and 0.25) during 30 seconds each. The region of interest of the half model, defined in the frame of the benchmark, is a 1.05 m x 1.45 m observation plane at a distance of y = 1.045 m (position of the wing root) from the microphone array.

Three grid resolutions of the source maps have been proposed in the frame of the benchmark: 1 cm, 2 cm and 5 cm leading to different numbers of equidistant scanning points respectively of 15476,

3869 and 660.

In this paper, results for the case of M=0.25 (88m/s) and 3° angle are presented, for a grid of 2 cm resolution (3869 points).

3.2 Algorithms monitoring

The adopted mode of analysis of all the results begins with the observation of the source power by area. Indeed, in general, we observe a relatively rapid convergence on these quantities [4]. We then deduce a number of iterations that could be considered as sufficient or satisfying a convergence criterion (to be determined). We note that the source powers by area are quite coherent between them from one algorithm to another. Then we observe the criteria L0, L1 and L2 (calculated on the source map at each iteration) and finally the relevant criteria on the value of the functional and on the residue.

Not surprisingly, two groups of algorithms are identified. The first (view as a L2-norm class of algorithm) composed of CG (SEM), CIRA and NNLS (very close but with NNLS a little more sparse) and DAMAS (even more sparse) and the other group (view as a L1-norm class of algorithm) composed of Clean-PSF which provides the sparsest maps (often impossible to visualize). The degree of sparsity is observed with criterion L0 which always decreases for the first group and always increases for the second, as expected. Thus, CG(SEM), CIRA and NNLS find a variable number of sources depending on the frequency. This is not the case for DAMAS and Clean-PSF (see Figure 1).

Figure 1 – Evolution of criteria L0-norm (left) and L1-norm (right) over frequencies at a converge state (judged as such).

L0-norm criterion is never used as an exit conditions of a deconvolution algorithm as far as we know. Although imposing a number of lighted source points is difficult to conceive for engineers, the number of sources being unknown *a priori* and can be one of the unknowns of the problem, we observe a great similarity of the visual representation by doing so. Figure 2 shows maps calculated at 8496Hz imposing a number of visible source around 360 (determined according to the power level dynamics) for CG(SEM), CIRA and NNLS algorithms. It is interesting to note then that the number of iterations is quite different, respectively 100, 26 and 10. This highlights the intrinsic tendency to sparsity of each algorithm.

Criterion L1 is interesting to observe: there is generally fast convergence towards a stable value but whose value depends on the frequency. Similarly, criterion L2 is always increasing with asymptotic behavior. It's interesting regarding the number of sources: for the first group the more iterates, the less we have enlightened source points, the more we tend towards sparsity but the energy of the map increases slightly. We therefore operate a concentration of energy on identified source points. For the other criteria, we observe a relatively good consistency of the ε criterion for DAMAS and $L2nr$ for CG(SEM), CIRA, NNLS and even Clean-PSF. But the evidence is less clear than for L1-norm criteria.

Generally, we therefore observe the regularizing effect and the tendency to sparsity of the positivity constraint with a gradation toward sparsity from CG(SEM), CIRA, NNLS, DAMAS to Clean-PSF. In our view, the effect is essentially of the order of the visualization of the maps because the powers per areas are consistently estimated between the 5 algorithms.

The analysis of those criteria showed that it is difficult to define common thresholds for all algorithms and each energy criterion defined in §2.5.1. However the evolution of the criteria over iterations seemed more suited to that. Thus we finally selected commonly to the 5 algorithms three criteria and defined three thresholds constant on the frequency band. Indeed, the intention was to drive the algorithms in the most unified way and the thresholds have been chosen the least restrictive so as to be suitable for all algorithms over a wide frequency band. The choice of the three criteria was based on the greatest representativeness of the quantities of interest of the problem (refer to §2.5.1): adequacy of the model to the measurement on the array ($\left|\varepsilon^{(i)} - \varepsilon^{(i-1)}\right|$), source map energy considering

the physical quantity of interest ($\left|L1n^{(i)} - L1n^{(i-1)}\right|$) and minimization of the residue error in the convolution problem ($\left|L2nr^{(i)} - L2nr^{(i-1)}\right|$).

Then it has been possible to roll out the calculations throughout the complete frequency band.

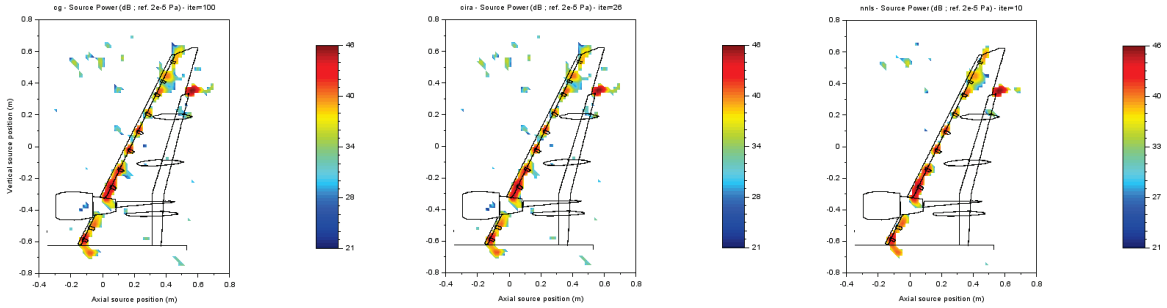

Figure 2 – Comparison of maps obtained using CG(SEM) (left), CIRA (middle) and NNLS (right) algorithms by imposing a fixed number of lighted source points (~360) at 8496Hz.

3.3 1/3 octave calculation analysis

Calculations were done on the third octave bands from 2kHz to 8kHz, monitoring the source power levels on the three areas defined on the map (FLAP INT, SLAP INT and FLAP TIP), the average iteration number and the average CPU time each per third octave band.

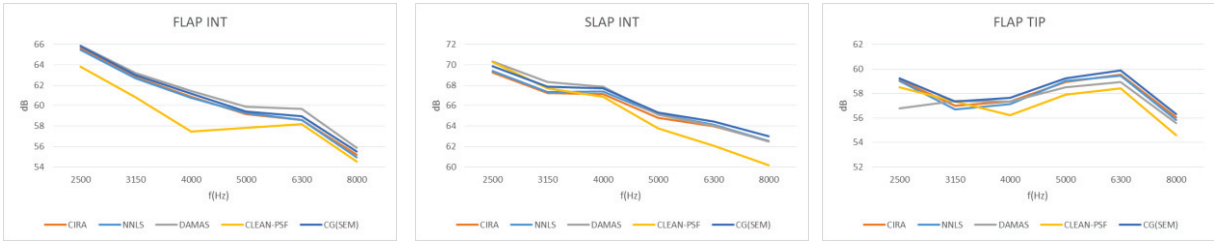

Figure 3 – Source power level par area (FLAP INT left, SLAP INT in the middle and FLAP TIP in the right).

The behavior already observed during fine-band calculations for monitoring (§3.2) is confirmed with third octave calculations: the source power level per area is quite well uniformly founded by each algorithms (figure 3), within the range of few dBs, while the visual representation of the source map is very different, highlighting the nature of each algorithm in terms of sparsity representation of the sources. Only the CLEAN-PSF algorithm deviates from the general trend. We believe that this is not due to the intrinsic nature of the algorithm, its natural tendency to sparsity (L1-norm class of algorithm). The experience gained during this study indeed encourages us to think that the iteration number is not enough high. In other words, the exit conditions defined in a common way to all the algorithms are not restrictive enough for this algorithm. It may well be that the differentiation of the algorithms adopted in this work (L2-norm class vs. L1-norm class) is not valid in the end.

Concerning the average iteration number and the average relative CPU time per third octave band observed during calculations, we see that they are relatively independent of frequency excepting for DAMAS. Note that CPU time is calculated relatively to the CBF CPU time calculation. The monitoring also indicates that sparsity of the source model has a computational cost.

4. CONCLUSIONS

With the aim of classifying the microphone array deconvolution methods in aeroacoustics, a common protocol for controlling and monitoring the different algorithms selected has been defined and applied to a use case taken from the Array Analysis Benchmark (DLR1).

We actually observe that the necessary positivity constraint of the deconvolution problem considered here has a strong regularizing effect and tends to foster sparsity of the solution. Thus the 5 selected algorithms coming from applied mathematics find equivalently sound power levels on areas defined in the source map for industrial analysis process, both in fine band as in third octave band. This is a comforting result that must convince engineers that when we want to solve an inverse problem, the most important is not the choice of the algorithm as such but rather the way we define the inverse problem and the way the algorithm is controlled. Thus the classification of the algorithms

deduced from this work lies in the sparsity of the obtained source model (and of its consequence in terms of visual representation) and in the computation time. The intuition of the classification of the algorithms on the Lp-norm nature is not demonstrated, for the selected algorithms and with the applied protocol.

The importance of the algorithm exit conditions is highlighted through this work. The intention to drive the algorithms in the most unified way (on the threshold choice at least) probably does not make much sense except for the demonstration proposed here. A more rigorous study of the convergence of the deconvolution algorithms should be done now.

Finally, we must also keep in mind that the observation conducted in this work may probably be strongly linked to the test case itself. Thus for a generalization of the conclusions, it is necessary to apply this protocol to others aeroacoustic use cases.

ACKNOWLEDGEMENTS

The authors wish to acknowledge the array methods community for their input with regard to the value of this work, selecting datasets of interest, defining metrics, and providing feedback at various meetings and additionally, they wish to thank the team at DLR DNW-KKK facilities for their efforts in acquiring data for analysis.

This work was conducted in the frame of the Labcom P3A (ANR-13-LAB2-0011-01).

REFERENCES

1 J. Billingsley et R. Kinns, «The Acoustic Telescope,» Journal of Sound and Vibration, vol. 48, 1976.

2 D. H. Johnson et D. E. Dudgeon, Array Signal Processing: Concepts and Techniques, Prentice Hall, 1993. 0-13-048513-6, 1993.

3 R. Dougherty et W. Stoker, «Sidelobes supression for phased array aeroacoustic measurement,» chez AIAA/CEAS 1998-2242, 1998.

4 T. F. Brooks et W. M. Humphreys, «A deconvolution approach for the mapping of acoustic sources (DAMAS) determined from phased microphone arrays,» Journal of Sound and Vibration n°294, p. 856–879, 2004.

5 D. Blacodon et G. Elias, «Level estimation of extended acoustic sources using a parametric method,» Journal of Aircraft, vol. 41, n° %16, pp. 1360-1369, 2004.

6 P. Sijtsma, «CLEAN Based on Spatial Source Coherence,» International Journal of Aeroacoustics, n° %16, pp. 357-374, 2007.

7 K. Ehrenfried et L. Koop, «Comparison of Iterative Deconvolution Algorithms for the Mapping of Acoustic sources,» AIAA Journal, vol. 45, n° %17, p. 1584, 2007.

8 G. Elias, «Experimental Techniques for Sources Location,» Von Karman Institute for Fluid Dynamics, VKI LS 1997-07, Aeroacoustic and active noise control., 1997.

9 T. Ahlefeldt, «Aeroacoustic measurements of a scaled half-model at high Reynolds numbers,» AIAA Journal, vol. 51, n° %112, pp. 2783-2791, 2013.

10 C. J. Bahr, W. M. Humphreys, D. Ernst, T. Ahlefeldt, C. Spehr, A. Pereira, Q. Leclère, C. Picard, R. Porteus, D. J. Moreau, J. Fischer et C. J. Doolan, «A comparison of microphone phased array methods applied to the study of airframe noise in wind tunnel testing,» chez 23rd AIAA/CEAS Aeroacoustics Conference, 2017.

11 Q. Leclère, A. Pereira, C. Bailly, J. Antoni et C. Picard, «A unified formalism for acoustic imaging based on microphone array measurements,» International Journal of Aeroacoustics, vol. 16, n° %14-5, pp. 431-456, 2017.

12 A. Finez, C. Picard, T. Le Magueresse, Q. Leclère et A. Pereira, «Microphone array techniques based on matrix inversion,» Von Karman Institute for Fluid Dynamics, VKI Lecture Series STO-EN-AVT-287-05, 2017.

13 C. Picard, F. Lepercque, T. La Magueresse, O. Minck, R. Hallez et J. Lanslots, «Microphone Array Deconvolution Methods for Efficient Aeroacoustic Testing in Wind Tunnels,» chez Inter.Noise 2019, Madrid, 2019.